Modeling of Air-Fuel Ratio Dynamics of Gasoline Combustion Engine with ARX Network

Tomáš Polóni

Institute of Automation, Measurement and Applied Informatics,

*Faculty of Mechanical Engineering, Slovak University of Technology, Bratislava, Slovakia**

Tor Arne Johansen

Department of Engineering Cybernetics,

Norwegian University of Science and Technology, Trondheim, Norway

Boris Rohaľ-Ilkiv

Institute of Automation, Measurement and Applied Informatics,

Faculty of Mechanical Engineering, Slovak University of Technology, Bratislava, Slovakia

Abstract

The article deals with nonlinear modeling of air-fuel ratio dynamics of gasoline engines during transient operation. With a collection of input-output data measured near several operating points of the commercial engine we have identified a global model of the system. The global model structure comes out of the modeling principles based on a weighting of local linear ARX model parameters in dependency of the operating point. It was found that the studied global model has the ability to approximate nonlinear effects and varying response time as well as varying time delay of air-fuel ratio dynamics. The advantage of the local linear approach is that it is flexible to fit experimental data and provides an appropriate structure for advanced nonlinear control algorithm synthesis. Moreover, the proposed nonlinear AFR model with identified numeric values of parameters listed in this article can be used for simulation purposes and also for testing of control algorithms.

Keywords: air-fuel ratio, weighted local linear ARX models, weighting function

*Electronic address: `tomas.poloni@stuba.sk`

I. INTRODUCTION

The problem of air-fuel ratio (AFR) control is one of the main parts of the more complex emission reduction strategy for combustion engines. The mixture quality is essential for efficiency of a three-way catalytic converter and therefore sufficient control techniques are needed to fulfil emission legislations.

During the last twenty years nonlinear control methodologies were developed from simple to more sophisticated "model (observer)-based" ones. In advanced control methods the model plays the most important role. A classical approach to modeling problem of AFR is based on linear observer theory where physical models of the process are a part of a state estimator [7] [23]. A great focus was pointed to the first principle Mean Value Engine Models that in a detailed physical approach describe the individual engine parts, e.g. the filling and emptying of intake manifold [9], the wall wetting phenomena [2, 21] and the residual gas fraction dynamics together with the mixing dynamics [17]. A review of observers, based on physical laws related to "gray-box" models, can be found in [10].

Another promising branch of control model-based strategies relies on "black-box" modeling principles where identified models are used. Many different nonlinear model structures have been applied to engine emission control problems from the field of nonlinear approximation theory. One of the most popular approaches to combustion engine modeling is based on neural network principles for their flexibility [20]. Especially, the AFR modeling problem was solved by radial basis function observer [18, 25], by Chebyshev polynomial network [6] and recently a simulator of AFR dynamics based on recurrent neural network was proposed by Arsie et al. [3]. The standard problem of modeling at the air-path is the ability to estimate the momentary amount of inflowing air to the cylinders as an unmeasurable quantity. The inflowing air into the cylinders has been computed with the neural estimator [15]. For the same purpose, the air-path fuzzy model with the application of clustering algorithm is designed in [4], where the model is able to cover the required operating space of the engine. The neural network model of AFR, identified from experimental data, is proposed in [1]. Such a model, contrary to the previously mentioned, models the AFR directly in the exhaust manifold. An unconventional method of the control and modeling is mentioned in [22], where they are not searching for exact model of the AFR dynamics, but they aim directly to identify the parameters of the controller. In their case the solution has been reduced to

parametric system identification problem.

The purpose of this study is to identify a suitable model for nonlinear model-based control strategy and to verify its ability to deal with nonlinear parameter varying AFR dynamics during transient operation. This paper discusses an open loop identification procedure of AFR on an 2.8 liter engine. Specifically, composite local linear ARX models with weighted validity [19] are identified to model AFR nonlinear dynamics. The global AFR model is then validated against the measured data. Weighted linear local models (LLM) have already been used in engine emission NOx control applications as an extension of radial basis function network sometime referred to as local linear neuro-fuzzy tree network [11] [8] as well as in diesel engine drivetrain modeling [13]. Compared to its alternatives, the benefit of weighted ARX model approach is in its modularity and simple augmentation with the LLM from different operating regimes.

II. MODEL STRUCTURE AND IDENTIFICATION

This section closely describes the model structure together with the identification process. First, a general weighted linear local model with single input single output (SISO) structure is presented. Then, it is shown how such a structure can be applied for modeling and identification of AFR dynamics. In the final part the design of weighting functions and experimental results are presented.

A. Weighted Linear Local Model Network Structure

The basic principle of this nonlinear modeling technique lies in partitioning the operating range into operating regimes. For these operating regimes LLMs are defined. The transition between particular local models is fluent because of smooth interpolating validity functions.

The local models mentioned here will be linear ARX models, e.g. [16], with weighted parameters depending on the operating point $\phi \in \Phi \subset \mathbb{R}^{n_\phi}$

$$\sum_{h=1}^{n_M} \rho_h(\phi(k))A_h(q)y(k) = \sum_{h=1}^{n_M} \rho_h(\phi(k))B_h(q)u(k) + \sum_{h=1}^{n_M} \rho_h(\phi(k))c_h + e(k) \tag{1}$$

Polynomials A_h and B_h are defined by

$$\begin{aligned} A_h(q) &= 1 + a_{h,1}q^{-1} + \ldots + a_{h,n_y}q^{-ny} \\ B_h(q) &= b_{h,1+d_h}q^{-1-d_h} + \ldots + b_{h,n_u+d_h}q^{-nu-d_h} \end{aligned} \tag{2}$$

where $a_{h,i}$,$b_{h,(j+d_h)}$,c_h are the h-*th* local model parameters and d_h is a transport delay of the local model. The output from the system is $y(k)$ and the input $u(k)$. In general, we assume the stochastic term $e(k)$ in Eq. (1) to have a white noise properties. The parameter n_M stands for the number of local models, and q^{-1} is the time shift operator, i.e. $q^{-i}y(k) = y(k-i)$. The Gaussian local model validity function $\tilde{\rho_h} : \Phi \rightarrow (0,1)$ indicates the degree of validity of the h-*th* local model. It is defined by the vector of center $\mathbf{c}_{c,h} \in \mathbb{R}^{n_\phi}$ and by the scaling matrix $\mathbf{M}_h$

$$\tilde{\rho_h}(\phi) = e^{-(\phi-\mathbf{c}_{c,h})^T\mathbf{M}_h(\phi-\mathbf{c}_{c,h})} \tag{3}$$

$$\mathbf{M}_h = \begin{pmatrix} \frac{1}{\sigma_{h,1}^2} & 0 & \cdots & 0 \\ 0 & \frac{1}{\sigma_{h,2}^2} & \cdots & 0 \\ \vdots & \vdots & \ddots & \vdots \\ 0 & 0 & \cdots & \frac{1}{\sigma_{h,n_\phi}^2} \end{pmatrix} \tag{4}$$

The scaling matrix $\mathbf{M}_h$ is further defined by the scaling factors $\sigma_{h,i}$ which shape the validity function. To achieve a partition of unity, local model validity functions are normalised to get the weighting functions used

$$\rho_h(\phi) = \frac{\tilde{\rho_h}(\phi)}{\sum_{h=1}^{n_M}\tilde{\rho_h}(\phi)} \tag{5}$$

That means in any operating point $\sum_{h=1}^{n_M}\rho_h(\phi) = 1$. For simulation of the model Eq. (1), the following recursive equation is used

$$y_s(k) = \sum_{h=1}^{n_M}\rho_h(\phi(k))\left(-\sum_{i=1}^{ny}\hat{a}_{h,i}q^{-i}y_s(k) + \sum_{j=1}^{nu}\hat{b}_{h,(j+d_h)}q^{-j-d_h}u(k) + \hat{c}_h\right) \tag{6}$$

When the estimated parameter vector $\hat{\theta}_h$ and the regression vector $\gamma(k)$ are introduced

$$\hat{\theta}_h = [\hat{a}_{h,1}, \hat{a}_{h,2}, \ldots, \hat{a}_{h,ny}, \{0,0,\ldots,0\}_{d_h}, \hat{b}_{h,1+d_h}, \hat{b}_{h,2+d_h}, \ldots, \hat{b}_{h,nu+d_h}, \{0,0,\ldots,0\}_{d_{max}-d_h}]^T \tag{7}$$

$$\gamma(k) = [-y_s(k-1), -y_s(k-2), \ldots, -y_s(k-ny), u(k-1), u(k-2), \ldots, u(k-nu-d_{max})]^T \tag{8}$$

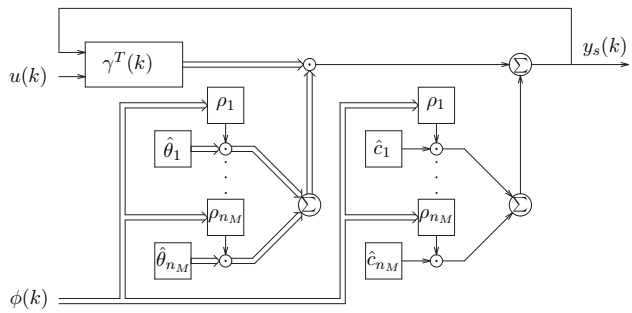

FIG. 1: Weighted ARX local model network structure

with $d_{max} = max\{d_h\}_{h=1}^{n_M}$, then Eq. (6) becomes

$$y_s(k) = \gamma^T(k) \sum_{h=1}^{n_M} \rho_h(\phi(k))\hat{\theta}_h + \sum_{h=1}^{n_M} \rho_h(\phi(k))\hat{c}_h \tag{9}$$

The offset term c_h of the local ARX model can be computed from the system's steady state values $y_{e,h}, u_{e,h}$. Given a parameter estimate $\hat{\theta}_h$, the estimate of c_h is defined as follows

$$\hat{c}_h = y_{e,h} + y_{e,h} \sum_{i=1}^{ny} \hat{a}_{h,i} - u_{e,h} \sum_{j=1}^{nu} \hat{b}_{h,j} \tag{10}$$

A block diagram illustrating Eq. (9) can be seen in Figure 1. There are several possibilities to estimate the parameters and weights of the model Eq. (1) [12]. This is going to be discussed in the next section for that particular problem. We will also get back to how the time-varying operating point $\phi(k)$ is defined and computed.

B. Air-Fuel Ratio Model Structure and Identification

1. *AFR Model Structure*

The dynamic model of AFR is based on a definition of a mixture as a ratio of air and fuel quantities in a time instance (k). Since the air-fuel ratio $\lambda(k)$ is non-dimensional, the air and fuel quantities can be expressed in any physical units, even the relative ones. It is convenient to express these quantities in the meaning of relative mass densities ($[g/cylinder]$) telling us how much mass of air (or fuel) is concentrated per volume of one cylinder. The relative mass density of a mixture consists of relative air density $m_a(k)$ and relative fuel density $m_f(k)$ that define the mixture quality in a time instance (k). The effect of mixture formation is

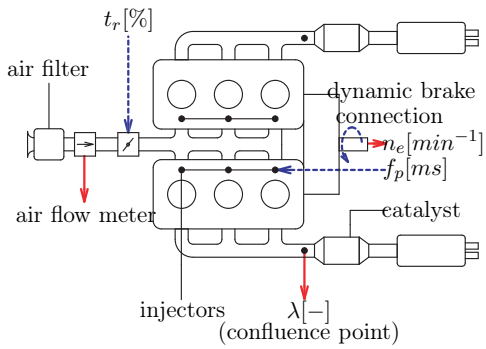

FIG. 2: Engine setup with input/output relations; dashed arrows - inputs, solid arrows - outputs

transformed from the discrete event process (one combustion cycle) to continuous changes of AFR information, due to mixing dynamics in the exhaust manifold. To scale the AFR at one for stoichiometric mixture ($\lambda_{st} = 1$), we divide the ratio by the value of theoretical stoichiometric coefficient for gasoline fuel $L_{th} \approx 14.64$. Thus the ratio is defined

$$\lambda(k) = \frac{1}{L_{th}} \frac{m_a(k)}{m_f(k)} [-] \tag{11}$$

The $m_a(k)$ and $m_f(k)$ information can be indirectly measured with a delay at the confluence point (Figure 2). For modeling $\lambda(k)$, two different subsystems with independent inputs have to be considered. In the air-path subsystem, the throttle position (t_r) input represents the disturbance variable (DV), and in the fuel-path subsystem, the fuel pulse width (f_p) input represents the manipulated variable (MV). The other DV is the engine speed (n_e) which is implicitly included in the model to define the operating point together with t_r. In accordance with the general model structure presented in section II A, the key variables are defined in Table I. In the operating point vector, the parameter δ represents the throttle position delay. To simulate the AFR dynamics, we combine Eq. (9) with Eq. (11)

$$\lambda_s(k) = \frac{1}{L_{th}} \left[\frac{\gamma_a^T(k) \sum_{h=1}^{n_A} \rho_{a,h}(\phi(k)) \hat{\theta}_{a,h} + \sum_{h=1}^{n_A} \rho_{a,h}(\phi(k)) \hat{c}_{a,h}}{\gamma_f^T(k) \sum_{h=1}^{n_F} \rho_{f,h}(\phi(k)) \hat{\theta}_{f,h} + \sum_{h=1}^{n_F} \rho_{f,h}(\phi(k)) \hat{c}_{f,h}} \right] \tag{12}$$

2. *Identification Procedure*

The estimation of local ARX model parameters is performed using the data from engine which are measured with an exhaust gas oxygen (EGO) sensor and with the air mass flow (AFS) sensor as a reference sensor. An open loop identification experiment is applied herein

TABLE I: Symbol connection between the general expression and the model

general symbol	air-path model	fuel-path model	operating point (model)
$y(k)$	$m_a(k)$	$m_f(k)$	
$u(k)$	$t_r(k)$	$f_p(k)$	
$\gamma(k)$	$\gamma_a(k)$	$\gamma_f(k)$	
$\hat{\theta}_h$	$\hat{\theta}_{a,h}$	$\hat{\theta}_{f,h}$	
$\rho_h(\phi(k))$	$\rho_{a,h}(\phi(k))$	$\rho_{f,h}(\phi(k))$	
$\hat{c}_h$	$\hat{c}_{a,h}$	$\hat{c}_{f,h}$	
$\phi(k)$			$[n_e(k), t_r(k-\delta)]^T$

for both subsystems isolating one type of dynamics from the other [14]. The dynamics of both relative mass densities can be measured indirectly. The experiment always starts from the stoichiometric steady state value in a given operating point ϕ. During the experiment the speed of the engine is kept constant. To excite the air path dynamics we have applied a pseudo random binary excitation signal (PRBS) to the throttle and have recorded the AFR signal, keeping the fuel pulse width (FPW) at the constant level, for which the AFR in steady state was stoichiometric (λ_{st}). With a constant FPW we have delivered the constant relative fuel density $m_{f,e}$. For the fuel path dynamics a similar procedure can be applied but with the throttle position fixed, and with constant relative air density $m_{a,e}$. After both experiments are completed with the air-path AFR data ($\lambda_a(k)$) and the fuel-path AFR data ($\lambda_f(k)$), we can compute the data for relative mass densities in a local operating point

$$m_a(k) = m_{a,e}\lambda_a(k) \tag{13}$$

$$m_f(k) = \frac{m_{f,e}}{\lambda_f(k)} \tag{14}$$

The magnitude of the PRBS should be designed in such a way that the mixture is always capable of igniting if the AFR is lean or rich. The design of the PRBS will be discussed in the next section.

Standard identification algorithms can be applied to estimate the parameters of linear ARX models [24] for both subsystems. In the chosen operating point with N observations

of input-output data, the prediction error for local air-path ARX model is defined as

$$\varepsilon_a(k, \theta_a) = \Delta m_a(k) - \Gamma_a^T(k)\theta_a \tag{15}$$

where

$$\Gamma_a(k) = [-\Delta m_a(k-1), \ldots, -\Delta m_a(k-ny), \Delta t_r(k-1-d), \ldots, \Delta t_r(k-nu-d)]^T \tag{16}$$

$$\theta_a = [a_1, \ldots, a_{ny}, b_{1+d}, \ldots, b_{nu+d}]^T \tag{17}$$

$$\Delta m_a(k) = m_a(k) - m_{a,e} \tag{18}$$

$$\Delta t_r(k) = t_r(k) - t_{r,e} \tag{19}$$

The estimate of the local ARX parameters can be computed by minimizing the prediction error in a least squares sense

$$\hat{\theta}_a = \arg\min_{\theta_a} \sum_{k=1}^{N} \varepsilon_a^2(k, \theta_a) \tag{20}$$

The optimal structure of local models among alternative candidates can be measured by the sum of squared residuals (SSR), with the N_v number of validation data

$$SSR_{s,a} = \sum_{k=1}^{N_v} \varepsilon_{s,a}^2(k, \hat{\theta}_a) \tag{21}$$

The SSR is computed using simulation rather than one-step-ahead prediction since the model is expected to be used for the nonlinear control design (Figure 3). Correspondingly, the simulation error for the LLM is defined as

$$\varepsilon_{s,a}(k, \hat{\theta}_a) = \Delta m_a(k) - \Delta m_{s,a}(k) \tag{22}$$

The estimate of the offset term has been computed with Eq. (10). The identification of fuel-path model is similar.

3. Local Model Identification Results

The experiments were performed with a commercial gasoline engine, having a displacement of 2771 cm^3 (Audi 2.8V6 30V). During the experiments the running engine had a coolant temperature of approx. 80°C . The air mass flow ($\dot{m}_a$) was measured at the beginning of the intake manifold with the AFS. The signal was integrated over one engine cycle

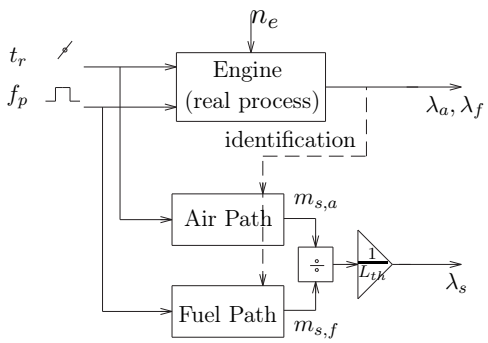

FIG. 3: Identification scheme of LLM

by which a steady state mass of air per one cylinder ($m_{a,e}$) was obtained. All output signals were sampled with a frequency 1 kHz, filtered with a low-pass filter, and down-sampled at the model sample period $T = 0.1s$. The engine was attached to a highly dynamic direct-current generator that can run in speed-controlled or torque-controlled mode. The generator can brake or drag the engine for possible emulation of the engine as a brake. The engine was not equipped with a turbocharger nor an exhaust gas recirculation system. The camshaft timing, together with the intake manifold volume, may be varied, however, in the presented experiments these were constant. The running of the engine and the engine control system in the lab were provided by a rapid prototyping system with Control Desktop software from the dSpace company. The software was running at the Axiomtec PC SBC8181VE. The following dSpace boards were used as the hardware interface: DS2002 AD/DA board, DS1103 AD/DA board, DS4003 digital I/O board, and DS1005 digital signal processing board. A special ICX-3 hardware interface [5] was placed between the engine and the PC. The function of ICX-3 is to exchange the data between the engine, which has the crank shaft dependent tasks (injection, ignition, etc.), and the control computer.

The identification experiments for both subsystems were performed in nine operating points. The measured operating points, defined by the steady state value $m_{a,e}$ and constant n_e, have been ordered from one to nine (OP1-9) (see Figures 6(b) and 7(b)). The measured validation data in comparison with the simulated LLMs for the air-path and the fuel-path in the first operating point are depicted in Figure 4 and Figure 5 respectively. For all LLMs the simulation error was found to be fairly low.

a. Air-Path The result of air-path identification is represented by the static characteristic (Figure 6(a)) and by the linear local models from dynamic measurements. The main

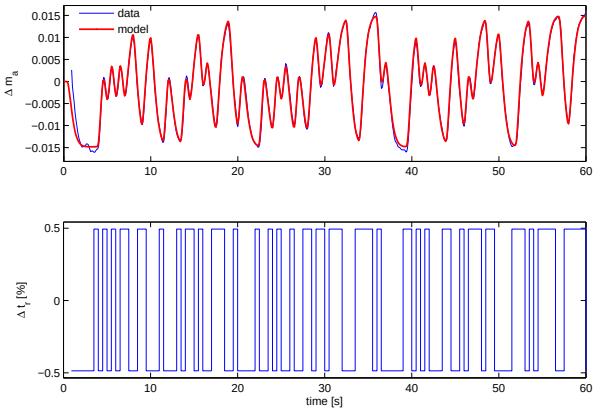

FIG. 4: Validation of ARX local model in the OP1; the air-path

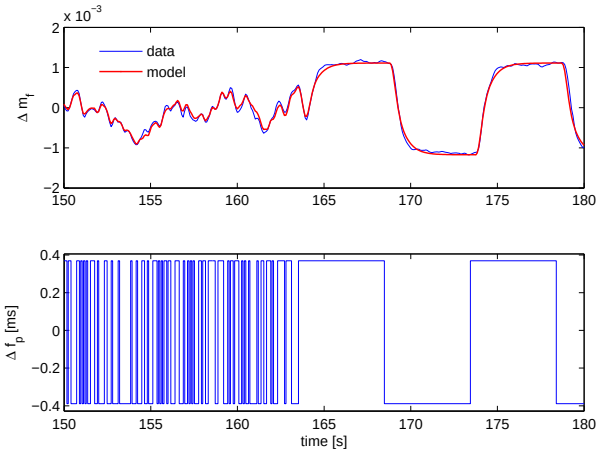

FIG. 5: Validation of ARX local model in the OP1; the fuel-path

nonlinearity of air mass flow is caused by the throttle. This is documented by the different identified gains of the LLMs in Figure 6(b). The static characteristic is a polynomial function of second order, with a constrained first derivative in operating points, that is fitted to the data to balance the gain information from static and dynamic measurements.

b. Fuel-Path The static characteristic identification of the fuel-path has shown that the system has almost identical gain in all investigated operating points (Figure 7(a)). This characteristic was also confirmed from the local model dynamic identification (Figure 7(b)). To simplify the fuel-path model, only the local models from operating points one, four and nine will be considered to represent the dynamics for the engine speed they have been

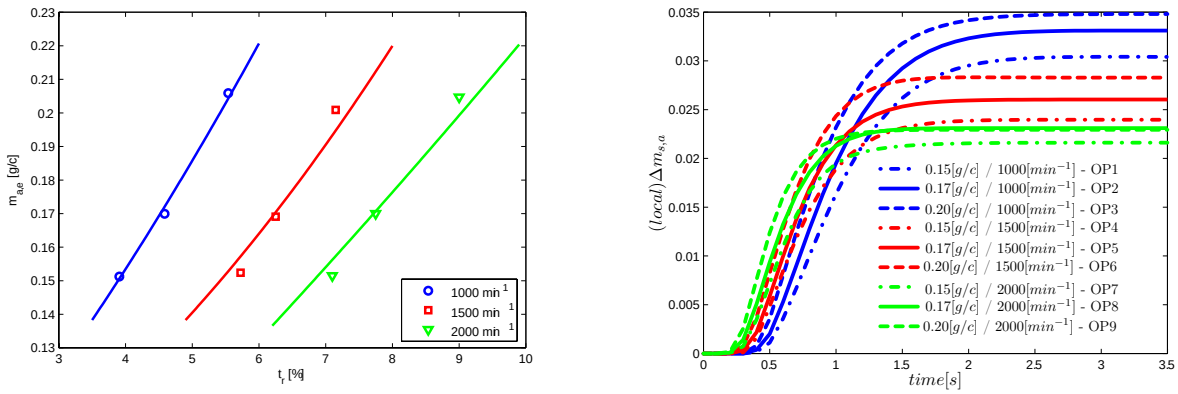

(a) Throttle vs. cylinder air static characteristic

(b) Step response of the local air path models in nine operating regimes

FIG. 6: The results of air-path identification

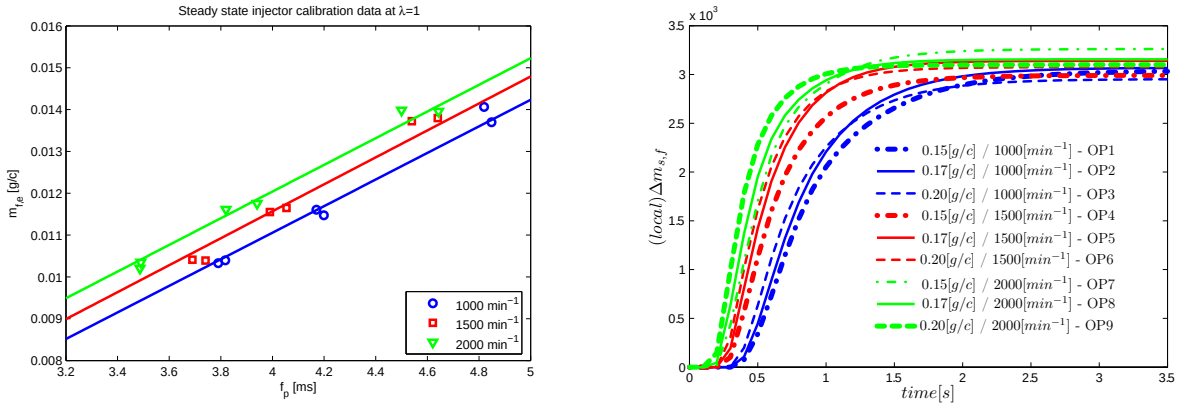

(a) Steady state injector calibration data at $\lambda = 1$

(b) Step response of the local fuel path models in nine operating regimes

FIG. 7: The results of fuel-path identification

identified for. Both subsystems showed varying time constants as dependent on the operating point.

4. *Weighting Function Design*

The local information about the AFR, with such a varying dynamics as the combustion engines have, is not enough to model the complex system. To bridge the local information through different operating points, the design of interpolation functions becomes important. A local weight function is associated with each LLM to define its validity. The local weighting

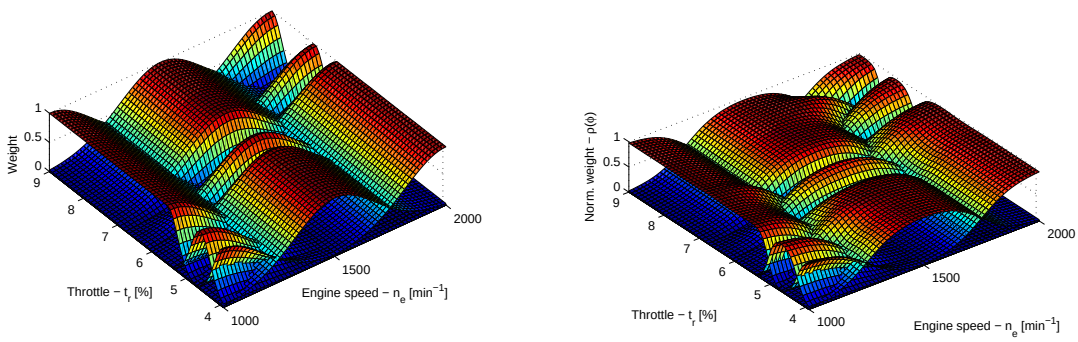

(a) Validity functions; the air-path

(b) Weighting functions; the air path

FIG. 8: Weighting functions used in the global AFR model; the air-path

functions can be chosen as any continuous functions. Their shape and extrapolation capacity into the areas, where no other local information is available, need to be considered. The presented Guassian functions defined in Eq. (3), with a vector of centers $c_c = [n_{e,e}, t_{r,e}]^T$, have this potential

$$\tilde{\rho}(\phi(k)) = \exp\left[-\begin{pmatrix}\Delta n_e(k) & \Delta t_r(k)\end{pmatrix}\begin{pmatrix}\frac{1}{\sigma_1^2} & 0\\ 0 & \frac{1}{\sigma_2^2}\end{pmatrix}\begin{pmatrix}\Delta n_e(k)\\ \Delta t_r(k)\end{pmatrix}\right]; \begin{cases}\sigma_2 = constant;\ interpolation\\ \sigma_2 = \infty;\ extrapolation\end{cases} \tag{23}$$

If the throttle position is within the operating range, where the LLM is extrapolated, then the parameter σ_2 is set to infinity. Otherwise it is a constant number. The tuning parameters (σ_1, σ_2) of validity function Eq. (23) for a given LLM were tuned to achieve smooth transition between different operating points. The weighting functions, as considered for the global AFR model are shown in Figures 8 and 9. The complete list of the identified parameters of all local linear models for both subsystems, together with the parameters of their local validity functions, can be found in the Appendix.

5. *Pseudo Random Binary Signal Design*

As to the type, more alternatives of the input excitation signal can be considered. Regarding the fact that we identify linearised models in a limited range of their operating points, the application of PRBS is technically simple to perform, since there are only two values to alter. Moreover, it is widely recognized that the PRBS is well suited for linear

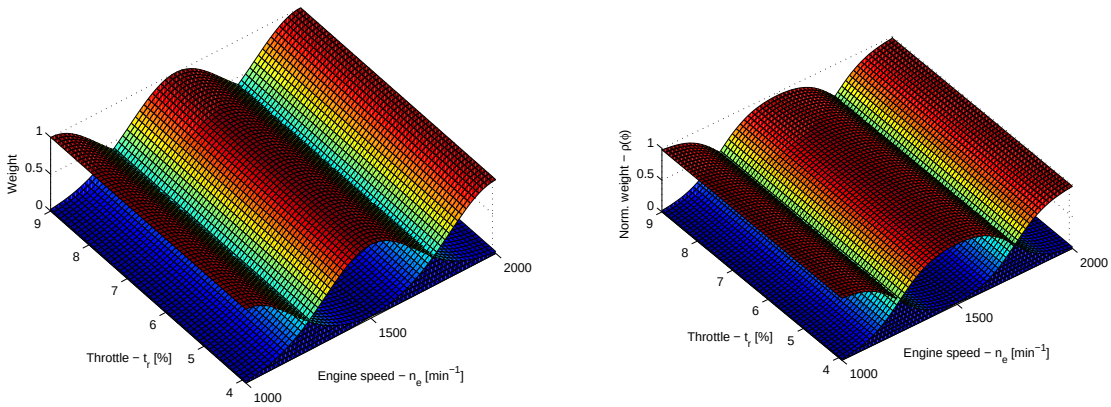

(a) Validity functions; the fuel-path

(b) Weighting functions; the fuel-path

FIG. 9: Weighting functions used in the global AFR model; the fuel-path

systems [16]. The multilevel random Gaussian signal and the swept sinusoid signal are the mentioned alternatives that could equally be used for this identification problem. To design the system identification experiment, we need to set the magnitudes and the order of the PRBS properly. Another parameter to consider is the integer ratio $n_r = T_c/T$, where T_c is the sample period for generating the PRBS (the clock period). In general, the magnitude of the PRBS is selected to maximize system output to noise ratio, and the order of the PRBS shall cover dominated frequencies of the identified system, so that these modes can be excited by the PRBS. The clock period is selected in such a way, that the actuator is able to respond to the PRBS command. For the design of the PRBS signal, two engine-time-period equations were assumed, specifically the time of four stroke cycle - T_{cyc} and the segment time - T_{seg}

$$T_{cyc} = \frac{i60}{n_e[min^{-1}]}[s] \tag{24}$$

$$T_{seg} = \frac{T_{cyc}}{n_{cyl}} \tag{25}$$

where i represents the number of crank shaft revolutions for one four-stroke cycle and n_{cyl} is the number of cylinders. It is necessary to point out that the clock period of PRBS signal should be greater than two times the engine segment time if the engine has two separate exhaust manifolds, as shown in Figure 2

$$T_c > 2T_{seg} \tag{26}$$

For a six cylinder four-stroke gasoline engine, the engine firing frequency (fuel injection, open intake valve) is $25Hz$ for one side of the engine at $1000min^{-1}$. The PRBS fuel excitation,

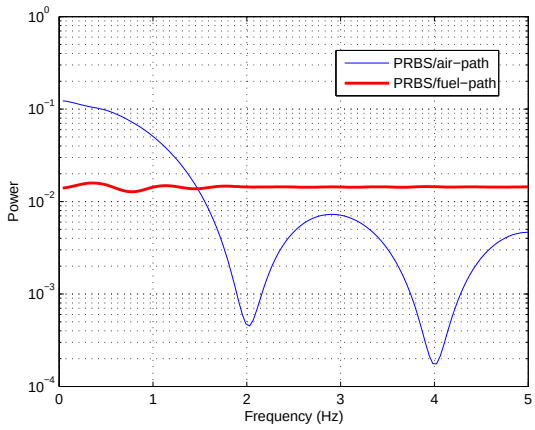

FIG. 10: Spectral density plot of the PRBS signals

generated at more than $25Hz$, will not be executed by one-side fuel injectors, providing a poorly identified model due to poor correlation between the fuel command input and the engine lambda output [26]. Figure 10 represents the power spectral density of the applied air-path PRBS with most of the power concentrated up to the frequency of 1.5 Hz, unlike the power of fuel-path PRBS that is distributed more uniformly. In Figure 10, the notch effect of spectral characteristic on the air-path PRBS is present. This is caused by low-pass filtering by increasing the clock period [16].

III. VALIDATION AND SIMULATION OF GLOBAL AFR MODEL

The validation of the global AFR model in a scope of full throttle disturbances requires a controlled fuel pulse width to keep the mixture quality in a range of physically acceptable limits suitable for ignition. Because the controller design is based on the identified model and is in the framework of continuing work, the global model is first validated against the local AFR data in all examined operating points. Both subsystems are validated separately, approx. in the range $0.9 < \lambda < 1.1$.

For the air-path model all identified LLMs have been included in the global model. The validation results are shown in Figure 11. In the fuel-path subsystem the local models from operating points one, four and nine were included into the global model to document the extrapolating ability of the local models. The model expectingly performs better in operating points from which the local model has been included in the global model. A

certain discrepancy between the data and the model can be seen in extrapolated operating points in Figure 12. A greater error was observed when extrapolating the global model into the operating areas for which the local models were not identified. Subsequently, the local model from OP1 was extrapolated into the area of engine operating points OP2 and OP3 (OP4 into OP5 and OP6; OP9 into OP8 and OP7). Furthermore, as shown for example in responses for $1000min^{-1}$: OP1, OP2, and OP3 in Figure 7(b), rather small difference in the parameters of the fuel-path model, will cause a substantial error in the OP2 and OP3 by the use of the nonlinear Eq. (11), as can be seen in Figure 12. We emphasize that the LLM from the OP1 is extrapolated into the operating regimes OP2 and OP3 which causes a priori a systematic error. The errors in OP2, OP3, OP5, OP6, OP7 and OP8 could only be reduced by an inclusion of the local models from these operating points into the global model. The aim of Figure 12 is to rationalize the inclusion of a local model and to document the influence of extrapolation upon the global simulation error.

A bias error of the global model is present as well. It is related to the estimate of the offset term Eq. 10. However, repeated steady state measurements can eliminate such error. The errors in Figure 11 and Figure 12 are basically induced by the limited structure of model in all operating points with just variable delay. Moreover, the application and set up of weighting functions themselves introduce certain error.

To see how the air/fuel-path models respond under varying speed conditions and greater excitations, synthetic input signals have been applied. Even though these simulations have only qualitative character, the results demonstrate the ability of the presented global structure to catch significant characteristics of nonlinear AFR dynamics in the tested operating points. The air-path simulation shows greater influence of changing speed conditions not only on the system gain, but also on the mean value of the signal $m_{s,a}$ (Figure 13). The result of fuel-path simulation is shown in Figure 14. The main significance of Figures 13 and 14 is to show how indirectly measurable components of λ quantity behave on the basis of identified local models. From the practical point of view these types of response can not be verified without an AFR controller being included.

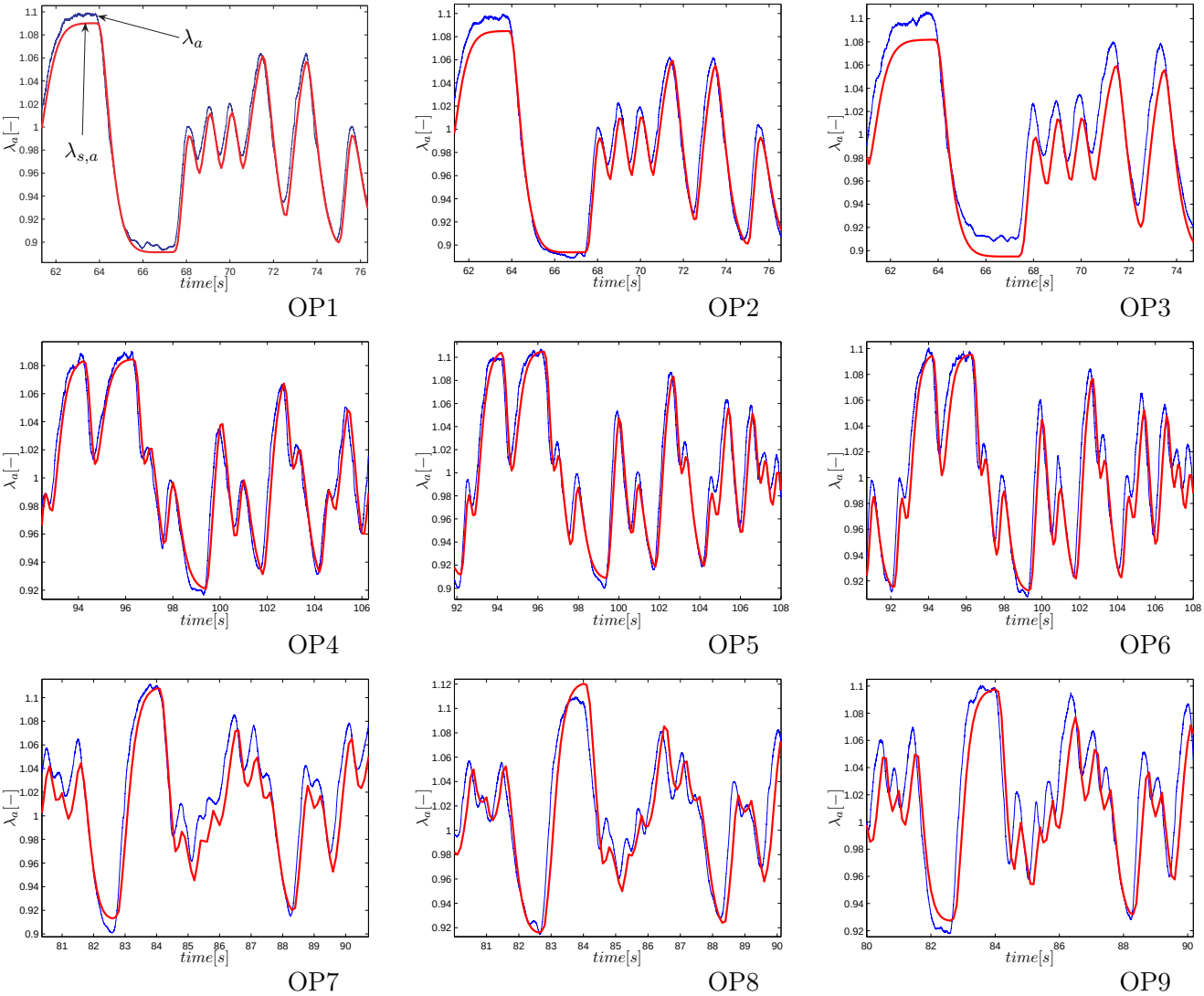

FIG. 11: Air-path validation of the global AFR model in the operating points (OP) 1-9

IV. CONCLUSION

In this article the ability of ARX local model network to model the nonlinear air-fuel ratio dynamics in a gasoline combustion engine was studied. The structure of the model as well as its identification procedure has been described alongside with the performance of the model as compared against validation data. It has been found that the studied global model, the parameters of which are listed in the Appendix, has the ability to approximate nonlinear effects and varying dynamics of air-fuel ratio.

The presented approach has also its limitations. Given methodology is applicable solely to those operating regimes, from which one can build the network of local models. For this

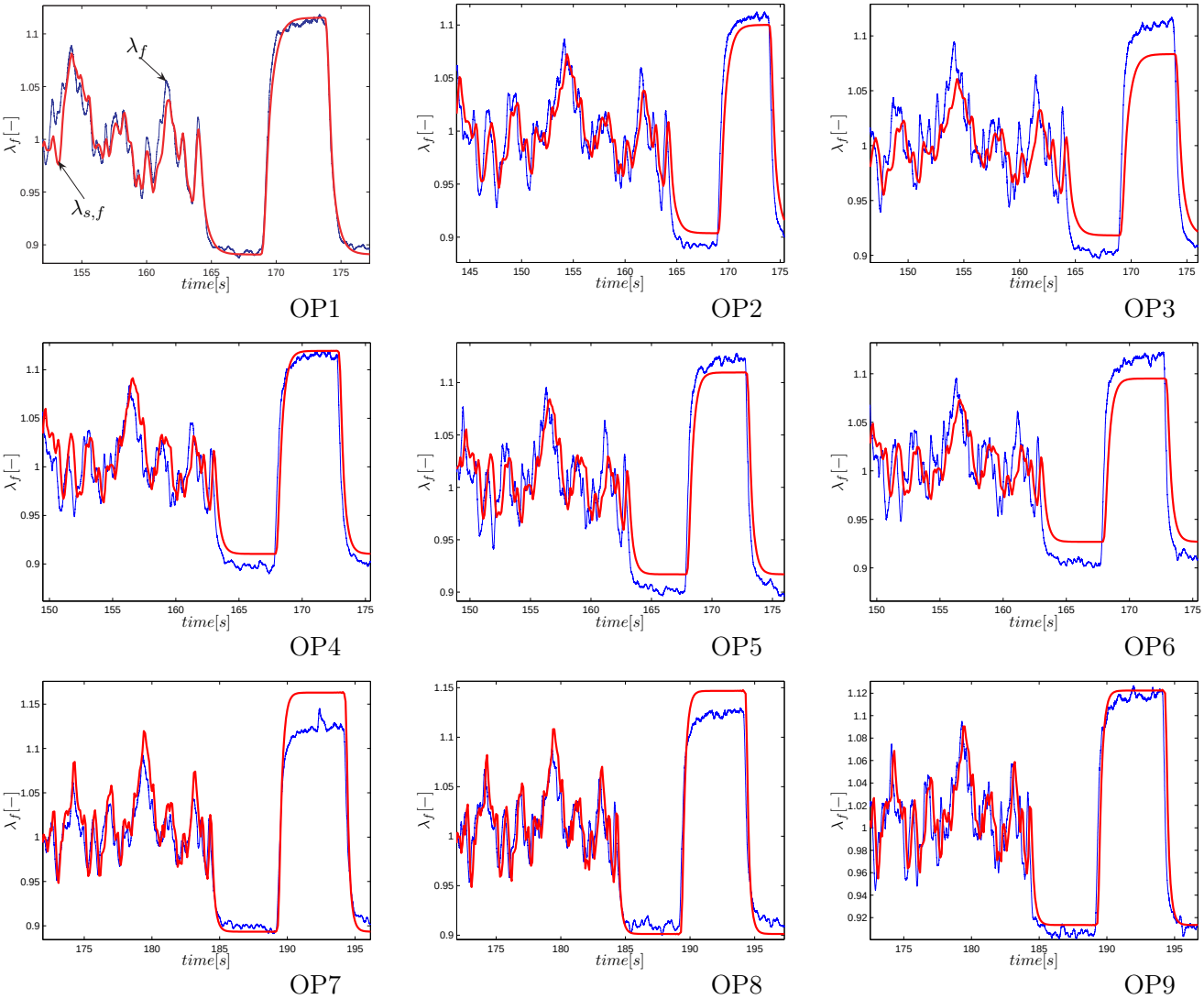

FIG. 12: Fuel-path validation of the global AFR model in the operating points (OP) 1-9

reason, the extrapolation capabilities are limited. Since the ageing of engine is still an issue it is necessary, from the engine lifetime point of view, to adapt the parameters of proposed model.

On the horizon of future work the nonlinear controller should be designed based on the proposed identified model extended to full operating range of engine.

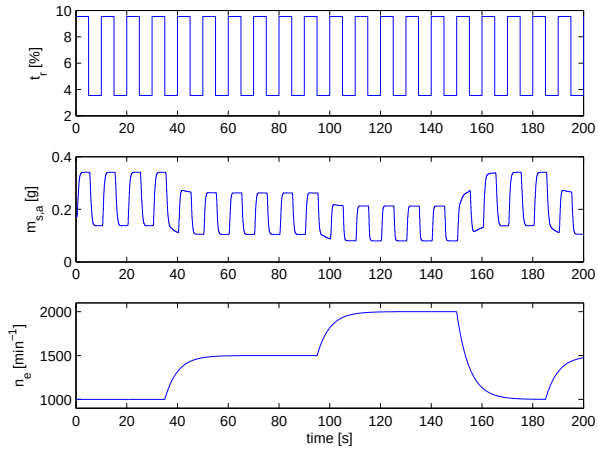

FIG. 13: Air-path simulation with the constant throttle steps

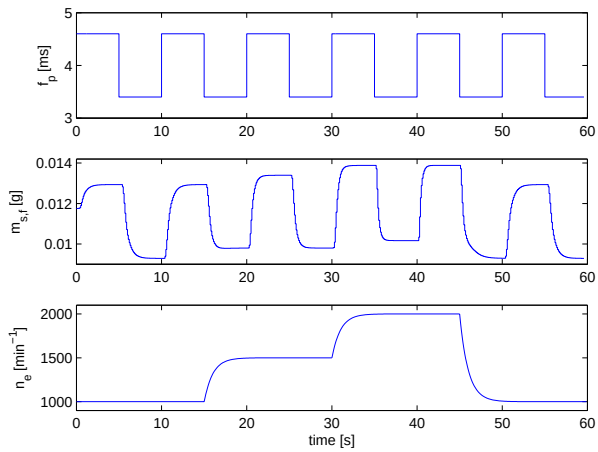

FIG. 14: Fuel-path simulation with the fuel pulse width modulation

Acknowledgments

T. P. acknowledges the support from Prof. L. Guzzella, Measurement and Control Laboratory-ETH Zürich, where the experiments on the gasoline combustion engine took place. This work was supported by the Slovak Research and Development Agency under the contract No. APVV-0280-06 and by Research Council of Norway: Strategic University Programme on Computational Methods in Nonlinear Motion Control.

TABLE II: List of air-path local model parameters

h, OP	$\hat{\theta}_{a,h} = [\hat{a}_{h,1}$	$\hat{a}_{h,2}$	$\hat{a}_{h,3}$	$\hat{a}_{h,4}$	$\hat{b}_{h,1}$	$\hat{b}_{h,2}$	$\hat{b}_{h,3}$	$\hat{b}_{h,4}$	$\hat{b}_{h,5}$	$\hat{b}_{h,6}]^T$	$t_{r,e}[\%]$	$m_{a,e}[g/c]$
1	-1.4537	0.4538	0.0799	-0.0137	0	0	0	0.0002	0.0007	0.0012	3.91	0.1507
2	-1.2971	0.2936	0.0660	0.0216	0	0	0	0.0004	0.0012	0.0013	4.585	0.1720
3	-1.1257	0.2442	-0.0941	0.0960	0	0	0	0.0008	0.0018	0.0015	5.54	0.2043
4	-1.2736	0.3672	0.0197	0.0063	0	0	0.0001	0.0013	0.0014	0	5.725	0.1572
5	-1.2644	0.3107	0.1142	-0.0364	0	0	0.0003	0.0014	0.0015	0	6.25	0.1704
6	-1.1543	0.2446	0.0368	0.0200	0	0	0.0008	0.0020	0.0014	0	7.15	0.1947
7	-1.5479	0.7297	-0.0204	-0.0527	0	0.0001	0.0006	0.0017	0	0	7.1	0.1562
8	-1.4022	0.6219	-0.0905	0.0064	0	0.0001	0.0012	0.0018	0	0	7.75	0.1707
9	-1.1570	0.4047	-0.0533	0.0090	0	0.0002	0.0022	0.0023	0	0	9	0.1993

TABLE III: List of fuel-path local model parameters

h, OP	$\hat{\theta}_{f,h} = [\hat{a}_{h,1}$	$\hat{a}_{h,2}$	$\hat{a}_{h,3}$	$\hat{b}_{h,1}$	$\hat{b}_{h,2}$	$\hat{b}_{h,3}$	$\hat{b}_{h,4}$	$\hat{b}_{h,5}]^T$	$f_{p,e}[ms]$	$m_{f,e}[g/c]$
1	**-1.8017**	**1.1704**	**-0.3010**	**[0**	**0**	**0**	**0.0746**	**0.1310]**.10^{-3}	3.7590	0.0103
2	-1.5684	0.8347	-0.1751	[0	0	0	0.1054	0.1744].10^{-3}	4.2180	0.0117
3	-1.4251	0.7061	-0.1621	[0	0	0	0.1980	0.1530].10^{-3}	4.9119	0.0140
4	**-1.3169**	**0.5716**	**-0.1094**	**[0**	**0**	**0.1012**	**0.3335**	**0]**.10^{-3}	3.7431	0.0107
5	-1.0977	0.3268	-0.0385	[0	0	0.1927	0.4056	0].10^{-3}	4.0210	0.0116
6	-0.9537	0.2151	-0.0271	[0	0	0.3027	0.4179	0].10^{-3}	4.5377	0.0133
7	-1.5649	0.9437	-0.2515	[0	0.0123	0.4029	0	0].10^{-3}	3.5715	0.0107
8	-1.2940	0.6310	-0.1544	[0	0.0447	0.5314	0	0].10^{-3}	3.8810	0.0117
9	**-0.9723**	**0.3213**	**-0.0719**	**[0**	**0.1436**	**0.7152**	**0**	**0]**.10^{-3}	4.4911	0.0136

APPENDIX: LIST OF IDENTIFIED PARAMETERS

The global AFR model can be built from the identified, and in this Appendix listed, numeric parameters of the local models for potential simulation, analyses or controller design. The identified parameters of air-path local models are summarized in Table II; Table III sums up the local models of fuel-path. The highlighted parameters of the local models (1,4,9) have been included in the fuel-path model. The parameters of validity functions are recorded in Table IV. The parameters in Table II (III) are noted in accordance to Eq. (7). For the computation of offset terms estimates $c_{a,h}$ ($c_{f,h}$) for each local model $h = 1-9$, it is necessary to pass $t_{r,e}, m_{a,e}$ ($f_{p,e}, m_{f,e}$) to Eq. (10).

TABLE IV: List of validity function parameters

		Air-Path σ_2		Fuel-Path σ_2
h, OP	σ_1 [a]	$t_r(k-\delta^b) \geq t_{r,e}$	$t_r(k-\delta) < t_{r,e}$	
1,4,7	260	0.4	∞	∞
2,5,8	260	0.4	0.4	∞
3,6,9	260	∞	0.4	∞

[a] This parameter is valid for both subsystems
[b] $\delta \approx 4-6$

[1] Alippi, C., C. de Russis and V. Piuri (2003). A neural-network based control solution to air-fuel ratio control for automotive fuel-injection systems. *IEEE Transactions on Systems, Man, and Cybernetics-Part C: Applications and Reviews* **33**(2), 259–268.

[2] Aquino, C. F. (1981). Transient a/f control characteristics of the 5 liter central fuel injection engine. *SAE Technical Paper No. 810494*.

[3] Arsie, I., C. Pianese and M. Sorrentino (2006). A procedure to enhance identification of recurrent neural networks for simulating air-fuel ratio dynamics in si engines. *Engineering Applications of Artificial Intelligence* **19**, 65–77.

[4] Copp, D. G., K. J. Burnham and F. P. Lockett (1998). Model comperison for feedforward air/fuel ratio control. In: *IEE UKACC International Conference on Control (Control'98)*. Swansea, UK.

[5] Geering, H. P., C. H. Onder, C. A. Roduner, D. Dyntar and D. Matter (2002). Icx-3 - a flexible interface chip for research in engine control. In: *Proceedings of the FISITA 2002 World Automotive Congress*. Helsinky. pp. 1–4.

[6] Gorinevsky, D., J. Cook and G. Vukovich (2003). Nonlinear predictive control of transients in automotive vct engine using nonlinear parametric approximation. *Transaction of the ASME (Journal of Dynamic Systems, Measurement, and Control)* **125**(3), 429–438.

[7] Guzzella, L. and C. H. Onder (2004). *Introduction to Modeling and Control of Internal Combustion Engine*. Springer.

[8] Hafner, M., M. Schuler and O. Nelles (1999). Dynamical identification and control of combustion engine exhaust. In: *Proceedings of the American Control Conference*. San Diego, Califor-

nia. pp. 222–226.

[9] Hendricks, E., A. Chevalier, M. Jensen, S. C. Sorenson, D. Trumpy and J. Asik (1996). Modelling of the intake manifold filling dynamics. *SAE Technical Paper No. 960037*.

[10] Hendricks, E. and J. B. Luther (2001). Model and observer based control of internal combustion engines. In: *Proc. MECA (Modeling, Emissions and Control in Automotive Engines)*. Salerno, Italy.

[11] Isermann, R. and N. Müller (2003). Design of computer controlled combustion engines. *Mechatronics* **13**(10), 1067–1089.

[12] Johansen, T. A. and B. A. Foss (1993). Constructing narmax models using armax models. *International Journal of Control* **58**(5), 1125–1153.

[13] Johansen, T. A., K. J. Hunt, P. J. Gawthrop and H. Fritz (1998). Off-equilibrium linearisation and design of gain-scheduled control with application to vehicle speed control. *Control Engineering Practice* **6**(2), 167–180.

[14] Jones, V. K., B. A. Ault, G. F. Franklin and J. D. Powell (1995). Identification and air-fuel ratio control of a spark ingnition engine. *Transactions on Control Systems Technology,IEEE* **3**(1), 14–21.

[15] Lenz, U. and D. Schroeder (1996). Artificial intelligence for combustion engine control. *SAE Technical Paper No. 960328*.

[16] Ljung, L. (1999). *System Identification: Theory for the User*. 2 ed.. Prentice Hall.

[17] Locatelli, M., C. H. Onder and H. P. Geering (2004). Exhaust-gas dynamics model for identification purposes. *SAE 2003 Transactions, Journal of Fuels and Lubricants, Paper No. 2003-01-0368*.

[18] Manzie, Ch., M. Palaniswami, D. Ralph, H. Watson and X. Yi (2002). Model predictive control of a fuel injection system with a radial basis function network observer. *Transaction of the ASME (Journal of Dynamic Systems, Measurement, and Control)* **124**, 648–658.

[19] Murray-Smith, R. and T. A. Johansen (1997). *Multiple Model Approaches to Modelling and Control*. Taylor&Francis.

[20] Nelles, O. (2001). *Nonlinear System Identification*. Springer.

[21] Onder, C. H., C. A. Roduner, M. R. Simons and H. P. Geering (1998). Wall-wetting parameters over the operating region of a sequential fuel-injected si engine. *SAE Technical Paper No. 980792*.

[22] Osburn, A. W. and M. A. Franchek (2004). Transient air/fuel ratio controller identification using repetitive control. *Transaction of the ASME (Journal of Dynamic Systems, Measurement, and Control)* **126**, 781–789.

[23] Powell, J. D., N. P. Fekete and C. F. Chang (1998). Observer-based air-fuel ratio control. *Control Systems Magazine,IEEE* **18**(5), 72–83.

[24] Söderström, T. and P. Stoica (1989). *System Identification*. Prentice Hall. New York.

[25] Wang, S. W., D. L. Yu, J. B. Gomm, G. F. Page and S. S. Douglas (2006). Adaptive neural network model based predictive control for air-fuel ratio of si engines. *Engineering Applications of Artificial Intelligence* **19**, 189–200.

[26] Zhu, G. George (2000). Weighted multirate q-markov cover identification using prbs-an application to engine systems. *Mathematical Problems in Engineering* **6**(2-3), 201–224.